

# Optimal Activation Function for Anisotropic BRDF Modeling

Stanislav Mikeš<sup>a</sup> and Michal Haindl<sup>b</sup>

*Institute of Information Theory and Automation of the ASCR, Pod Vodárenskou věží 4, Prague, Czechia*

**Keywords:** Anisotropic BRDF Models, Neural Network, Activation Function, BTF.

**Abstract:** We present simple and fast neural anisotropic Bidirectional Reflectance Distribution Function (NN-BRDF) efficient models, capable of accurately estimating unmeasured combinations of illumination and viewing angles from sparse Bidirectional Texture Function (BTF) measurement of neighboring points in the illumination/viewing hemisphere. Our models are optimized for the best-performing activation function from nineteen widely used nonlinear functions and can be directly used in rendering. We demonstrate that the activation function significantly influences the modeling precision. The models enable us to reach significant time and cost-saving in not trivial and costly BTF measurements while maintaining acceptably low modeling error. The presented models learn well, even from only three percent of the original BTF measurements, and we can prove this by precise evaluation of the modeling error, which is smaller than the errors of alternative analytical BRDF models.

## 1 INTRODUCTION

Visual scenes are predominantly represented with shapes and materials, and thus their recognition requires them to represent these properties realistically. Unfortunately, the surface material appearance considerably changes under variable observation conditions, which significantly negatively affects its automatic, reliable recognition in numerous artificial intelligence applications. As a consequence, most material recognition attempts apply unnaturally restricted observation conditions (Varma and Zisserman, 2009; Bell et al., 2015; Gibert et al., 2015). A surface material point representation that respects its appearance changes due to illumination and viewing conditions variations are the Bidirectional Reflectance Distribution Function (BRDF). A multi-dimensional visual texture is appropriate for a spatial surface reflectance function model. The best measurable representation is the seven-dimensional Bidirectional Texture Function (BTF) (Haindl and Filip, 2013). BTF can be simultaneously measured, even if it is not a trivial task, and modeled using state-of-the-art measurement devices and computers as well as the most advanced mathematical models of visual data. Features derived from such multi-dimensional BTF data models are information-preserving in the sense


that they can be used to synthesize data spaces closely resembling the original measurement data space.


The five-dimensional BRDF model obeys thirteen simplifying assumptions (Haindl and Filip, 2013) from the general reflectance model, among them non-negativity, energy conservation, and the Helmholtz reciprocity (von Helmholtz, 1867). Hence, the BRDF model depends only on five variables:

$$Y^{BRDF} = BRDF(\lambda, \theta_i, \phi_i, \theta_v, \phi_v), \quad (1)$$

where  $Y$  is a multispectral pixel,  $\lambda$  the spectral variable,  $\theta_i, \phi_i$  elevation and azimuthal illumination angles, and  $\theta_v, \phi_v$  are elevation and azimuthal viewing angles. Isotropic BRDF models represent materials whose reflections do not depend on the orientation of the azimuthal angles but only on their difference.

Several analytical isotropic (Minnaert, 1941; Phong, 1975; Blinn, 1977; Cook and Torrance, 1982; Strauss, 1990; Oren and Nayar, 1994; Ngan et al., 2005) as well as anisotropic (Torrance and Sparrow, 1966; Ward, 1992; Schlick, 1993; Lafortune et al., 1997; Ashikhmin and Shirley, 2000; Ragheb and Hancock, 2008; Dahlan and Hancock, 2016) BRDF models were proposed. The problem of reconstructing a measured isotropic BRDF from a limited number of BRDF-measured samples is addressed in (Nielsen et al., 2015). Another data-driven acquisition method of isotropic BRDF from two images was presented in (Xu et al., 2016). These models use only isolated pixel-based BRDF measurements and thus

<sup>a</sup>  <https://orcid.org/0000-0001-5741-8940>

<sup>b</sup>  <https://orcid.org/0000-0001-8159-3685>

reduce and less precise information than our proposed model, which learns from more informative and richer BTF data.

A neural BRDF model for joint estimation of reflectance and natural illumination from a single image of an object of known geometry was suggested in (Chen et al., 2021). Another neural network-based representation of BRDF data that enables the importance sampling of BRDFs was presented in (Sztrajman et al., 2021), but they use artifact-prone non-smooth activation function and less informative BRDF measurements.

Neural BRDF representation (Zheng et al., 2021) expresses BRDFs as continuous functions and allows importance sampling, but its extrapolation is poor. Neural BRDF model (Fan et al., 2021), which considers only isotropic materials, was applied to spatially-varying bidirectional reflectance distribution functions.

The isotropic BRDF models cannot represent materials with an anisotropic appearance faithfully (Ngan et al., 2005). However, most materials have an anisotropic appearance. Thus the isotropy is a severe limitation. Hence there is a need to develop novel, fully anisotropic BRDF models. The isotropic BRDF is a particular case of general anisotropic BRDF. Thus the presented model can faithfully model also any isotropic BRDF.

We propose a novel anisotropic deep neural net-based model for BRDF, which reliably learns BRDF model parameters from sparse BTF measurements. The NN model has numerous parameters, including network topology, initialization, optimizer, learning rate, loss function or angular representation, and others. Simultaneous optimization of all these free parameters is time-demanding. Thus, we have optimized the network topology and, subsequently, the activation function. We show that the activation function significantly influences the modeling precision. Our contribution is a novel anisotropic deep neural net-based BRDF model, model learning from more informative BTF measurements, and optimization of the activation function.

For our analysis in this paper, we take advantage of unique anisotropic UTIA BTF visual material measurements (Haindl et al., 2012; Haindl et al., 2015) detailed in the following section, and we can provide an accurate evaluation of modeling error.

## 2 BRDF MEASUREMENTS

The UTIA BTF database was measured using a high-precision robotic gonireflectometer (Haindl et al.,

Table 1: The number of used samples in training subsets.

$v \bullet i \bullet$	$ia$	$is$
$va$	$81 \times 81$ <b>100%</b> (6561)	$81 \times 14$ <b>17%</b> (1134)
$vs$	$81 \times 14$ <b>17%</b> (1134)	$14 \times 14$ <b>3%</b> (196)

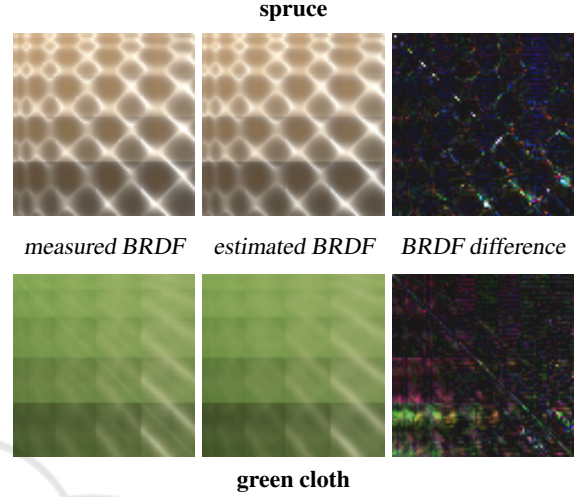


Figure 1: Spruce and cloth examples of the UTIA BTF database modeling results (models **15–30–20** with Soft-Sign,  $va-ia$ ). Error difference images are enhanced to become visible.

2012). The setup consists of independently controlled arms with a camera and light. Its parameters, such as angular precision of 0.03 degrees, the spatial resolution of 1000 DPI, or selective spatial measurement, classify this gonireflectometer as a state-of-the-art device. The typical resolution of the area of interest is around  $2000 \times 2000$  pixels, sample size  $7 \times 7$  [cm], sensor distance  $\approx 2$  [m] with the field of view angle  $8.25^\circ$  and each of them is represented using at least a 16-bit floating-point value for a reasonable representation of high-dynamic-range visual information. The illumination source is eleven LED arrays, each having flux 280 lm at 0.7 A, spectral wavelength  $450 - 700$  [nm], and have its optics. The memory requirements for storage of a single material sample amount to 360 gigabytes per color channel but can be much more for a more precise spectral measurement.

### 2.1 Measured BRDF

We measured each material sample in 81 viewing positions  $n_v$  and 81 illumination positions  $n_i$  resulting in 6561 images per sample (4 terabytes of data). We compute each BRDF value from its corresponding angular BTF measurement. These measured BRDF values, illustrated for spruce and green cloth in Fig. 1, we further use as the ground truth for the neural BRDF

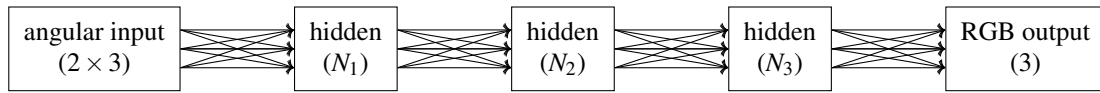


Figure 2: Neural network model.

model evaluation.

### 3 NEURAL NETWORK BRDF MODELS

We have experimentally verified neural models capable of accurately approximating unmeasured combinations of the illumination and viewing angles in the anisotropic BRDF space. Using cross-validation, the proposed model was selected from a set of simple deep neural models optimizing the BRDF modeling error Eq. (3). These simple models offer good modeling precision while simultaneously avoiding huge training set requirements, thus there is no need to use any complex state-of-the-art neural models. Our model (Fig. 2) starts with the view and illumination angles representation vector. Then several fully connected layers follow. The number of neurons in the hidden layers is 15–30–20, or 3–6–4 for a simpler model. The last (output) layer has three neurons corresponding to the RGB color. Except for the last layer, all neurons have one of the twenty selected activation functions (Fig. 3), and the last layer is linear. We implemented the neural network in the Tensorflow framework and designed it in a parallel way ( $81 \times 81$ ) to speed up training and prediction computations. The overall number of trainable parameters is 1268, or 88 for the simpler model. We used Glorot uniform initialization of weights, Adamax optimizer with a learning rate of 0.0025 and mean absolute error as the loss function. The models were trained for 500 epochs, and the times (Tab. 3–right) are measured on Tesla P100 / 16GB.

#### 3.1 Angle Representation

The view and illumination directions are described by spherical angles  $(\theta_v, \phi_v)$ ,  $(\theta_i, \phi_i)$ , where elevation / polar angle  $\theta_\bullet \in \langle 0, 90 \rangle$  and azimuthal angle  $\phi_\bullet \in \langle 0, 360 \rangle$ . We tested six different angle representations (e.g., Rusinkiewicz parametrization) for the input vector in our neural network model. The angle vectors are designed to overcome the discontinuity of azimuthal angle; the proposed formula for xyz representation follows:

$$\left[ \sin\left(\frac{\theta_v}{180}\right) \cdot \sin\left(\frac{\phi_v}{180}\right), \sin\left(\frac{\theta_v}{180}\right) \cdot \cos\left(\frac{\phi_v}{180}\right), \cos\left(\frac{\theta_v}{180}\right) \right].$$

Our estimation error results suggest the preferability to use xyz for angle vector representation.

#### 3.2 Activation Functions

We have selected the majority of published activation functions while excluding only some of their minor modifications. We have verified our assumption that non-smooth activation functions (Shamir et al., 2020) such as the Heaviside function, Piece-wise linear, Signum, ReLu, rReLu, SELU, HardTanh, HardShrink, SoftMax, SoftShrink, HardSigmoid are prone to create visual artifacts in areas around their non-smooth gradients. While authors (Shamir et al., 2020) searched for the average individual per-example class prediction difference over a set of models that are configured, trained, and supposed to be identical over some validation dataset, we aim to achieve modeling accuracy robustness to different training sets while simultaneously avoiding erroneous visual artifacts. Among the smooth activation functions (Shamir et al., 2020), ELU, Exponential, GELU, LiSHT, Mish, Sigmoid, SoftSign, Swish, Tanh, Snake, SoftPlus, and TanhShrink are searched for the most robust function which guarantees the best approximation accuracy for the wide range of sparse BTF measurements.

#### 3.3 Training Subsets

Fig. 4 shows spherical sampling over angular space. Two different angular subsets (*all*, *sixth*) are used to create learning sets for the neural network model. The training sets consist of texture patches with different views and illumination directions. Tab. 1 comprises the combinations of view and illumination subsets with the corresponding number of training patches and their relative size (concerning full measured space, i.e., 6561 patches).

## 4 RESULTS

The proposed BRDF model was trained using various subsets of the fully measured BTF texture space. For the experiments, we tested six wood veneers and nine other UTIA BTF material database materials. Two of them, the spruce veneer and green cloth, are illustrated here. The other thirteen materials confirm our conclusions. We tested four subset combinations

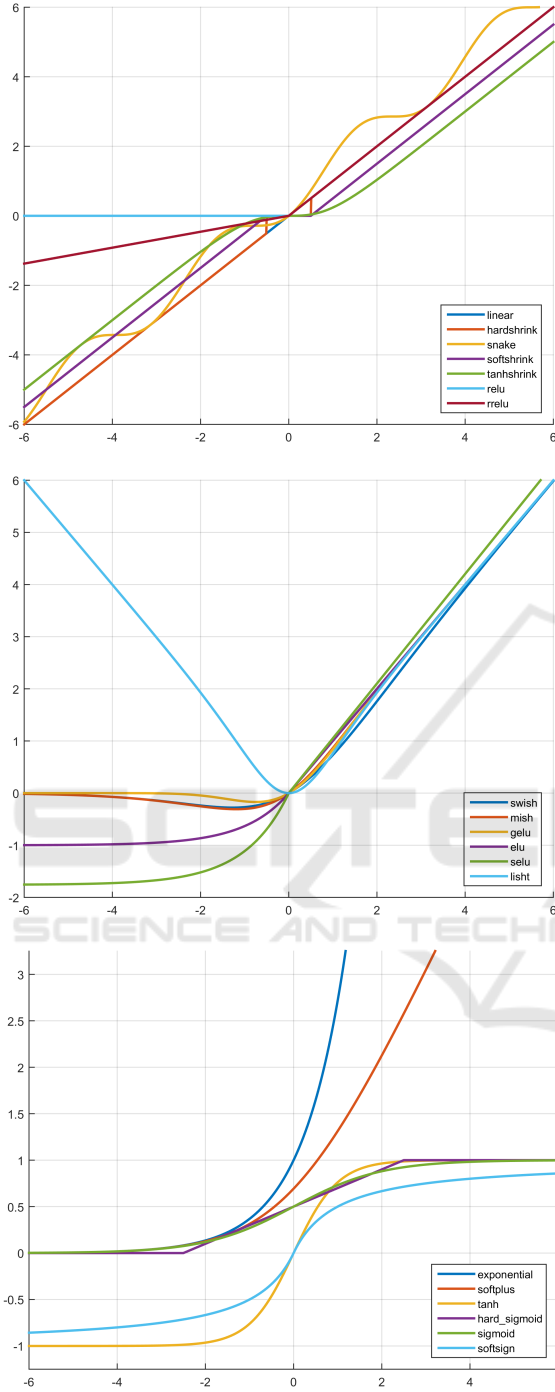


Figure 3: Nineteen of the tested activation functions (top – Linear, HardShrink, Snake, SoftShrink, TanhShrink, ReLU, rReLU; middle – Swish, Mish, GELU, ELU, SELU, LiSHT; bottom – Exponential, SoftPlus, Tanh, HardSigmoid, Sigmoid, SoftSign).

of viewing ( $v$ ) and illumination ( $i$ ) angles further denoted as  $(v/i)(a/s)$  (see Tab. 1).

The modeling quality is evaluated using the av-

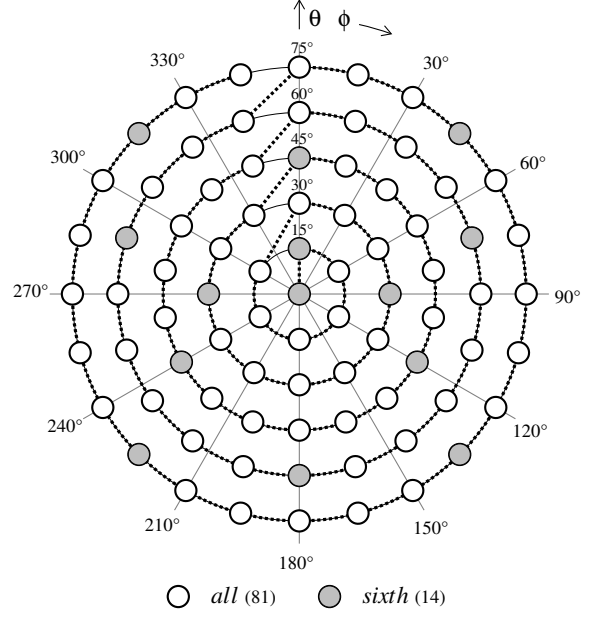


Figure 4: Angular subsets used for training – *all*, *sixth*.

erage absolute distance between the measured  $\beta(i, v)$  and estimated  $\tilde{\beta}(i, v)$  BRDF data:

$$\epsilon = \frac{1}{n_i n_v} \sum_{i=1}^{n_i} \sum_{v=1}^{n_v} |\beta(i, v) - \tilde{\beta}(i, v)| \quad (2)$$

where  $n_i, n_v$  are numbers of illumination and viewing angles. The spectral mean is the average

$$\bar{\epsilon} = \frac{1}{3} (\epsilon_R + \epsilon_G + \epsilon_B) \quad (3)$$

Tabs. 2,3 demonstrate the modeling quality results  $\bar{\epsilon}$  Eq. (3) for the color BRDF version. All errors are computed as a median interpolation error from five learned models. All spectral measurements are converted to 8 bits per spectral channel. The best activation function over all tested materials is SoftSign ( $f(x) = \frac{x}{|x|+1}$ ) followed by Tanh ( $\Delta\bar{\epsilon} = 0.48, \Delta = 9.4\%$ ), GELU ( $\Delta\bar{\epsilon} = 1.1, \Delta = 21.6\%$ ), ELU ( $\Delta\bar{\epsilon} = 1.13, \Delta = 22\%$ ), SELU ( $\Delta\bar{\epsilon} = 1.33, \Delta = 26\%$ )... SoftShrink ( $\Delta\bar{\epsilon} = 25, \Delta = 492\%$ ). The SoftSign average spectral error for 60 estimated NN-BRDF models (both models and both materials) is  $\bar{\epsilon}_s = 5.08$ ,  $\Delta\bar{\epsilon}, \%$  is the additive error for another activation function and its corresponding percentual increase. Visual quality comparison of these NN-BRDF models Fig. 5 confirms the same ordering and the visual defects produced by the non-smooth activation functions by their non-smooth functional parts. The non-smooth activation functions generate significant visible artifacts if mapped on curved object surfaces, and thus they cannot be used for realistic NN-BRDF modeling. These

Table 2: BRDF error  $\bar{\epsilon}$  (median from five) for spruce.



	15-30-20					3-6-4				
	<i>va-ia</i>	<i>vs-ia</i>	<i>va-is</i>	<i>vs-is</i>	$\emptyset$	<i>va-ia</i>	<i>vs-ia</i>	<i>va-is</i>	<i>vs-is</i>	$\emptyset$
LINEAR	23.92	23.99	24.01	24.25	24.04	23.94	23.98	24.13	24.24	24.07
SIGMOID	3.13	8.01	7.70	21.89	10.18	8.47	13.11	11.49	33.09	16.54
EXPONENTIAL	2.72	12.08	9.45	38.73	15.74	8.09	28.58	36.02	105.8	44.62
TANH	1.74	2.98	3.16	6.18	3.52	5.95	7.66	7.74	14.73	9.02
RELU	1.76	3.89	5.21	8.93	4.95	8.89	9.86	11.42	19.18	12.34
ELU	1.96	3.44	3.59	7.98	4.24	7.31	8.51	8.34	16.78	10.23
SELU	2.11	4.07	4.45	9.05	4.92	6.27	8.45	8.94	13.35	9.25
SOFTPLUS	2.32	9.84	10.78	14.91	9.46	9.13	12.03	13.32	21.66	14.03
TANHSHRINK	2.14	8.25	7.69	12.39	7.62	12.75	14.83	15.23	21.64	16.11
SOFTSIGN	1.59	2.58	2.77	5.01	2.99	5.54	8.01	7.99	11.72	8.31
HARDSHRINK	14.90	22.83	25.42	27.93	22.77	30.87	35.20	33.66	36.70	34.11
LISHT	1.71	5.24	6.10	11.24	6.07	7.59	8.61	15.03	15.31	11.63
SWISH	1.71	4.13	3.94	12.42	5.55	7.37	9.92	10.95	16.96	11.30
HARDSIGMOID	5.85	12.12	11.76	24.15	13.47	9.59	12.61	13.06	33.35	17.15
SNAKE	1.74	4.18	4.73	9.68	5.08	7.86	9.36	9.08	19.84	11.53
MISH	1.70	3.64	3.63	12.56	5.38	7.02	9.24	8.96	14.59	9.95
GELU	1.50	3.20	3.43	10.49	4.65	6.03	7.96	8.60	17.38	9.99
SOFTMAX	3.02	5.73	5.83	14.58	7.29	9.75	13.89	13.85	29.33	16.70
RRELU	1.79	2.98	3.67	7.73	4.04	7.50	9.39	13.16	17.24	11.82
SOFTSHRINK	35.96	35.96	36.05	36.05	36.01	35.96	35.97	36.03	36.05	36.00

Table 3: BRDF error  $\bar{\epsilon}$  and learning time for green cloth.

	error (median from five)					time [s] (avg. from five)			
	15-30-20		3-6-4		$\emptyset$	15-30-20		3-6-4	
	<i>va-ia</i>	<i>vs-is</i>	<i>va-ia</i>	<i>vs-is</i>		<i>va-ia</i>	<i>vs-is</i>	<i>va-ia</i>	<i>vs-is</i>
LINEAR	6.44	6.53	6.43	6.91	6.58	784	296	616	258
SIGMOID	2.86	5.84	4.48	15.84	7.25	857	318	646	256
EXPONENTIAL	2.21	14.42	4.45	16.71	9.45	858	317	647	259
TANH	2.14	4.49	3.90	6.07	4.15	859	319	647	258
RELU	1.87	5.38	4.47	6.42	4.53	860	319	649	260
ELU	2.25	4.32	4.12	5.86	4.14	869	320	641	256
SELU	2.19	6.83	4.24	6.95	5.05	872	320	643	258
SOFTPLUS	2.23	5.97	4.43	7.36	5.00	904	328	656	259
TANHSHRINK	1.97	5.90	4.43	11.21	5.88	974	352	670	270
SOFTSIGN	1.88	4.11	3.77	5.97	3.93	993	389	673	276
HARDSHRINK	17.31	18.40	18.15	18.66	18.13	998	386	673	277
LISHT	1.78	4.96	4.16	7.04	4.48	1015	353	680	270
SWISH	1.94	4.45	4.18	5.01	3.89	1045	352	685	265
HARDSIGMOID	3.48	5.94	4.47	16.07	7.49	1063	386	665	274
SNAKE	1.87	4.69	4.04	8.12	4.68	1110	427	695	282
MISH	1.88	4.31	4.10	6.25	4.14	1134	386	700	273
GELU	1.82	4.24	3.84	5.70	3.90	1248	426	716	277
SOFTMAX	2.31	5.81	4.93	6.12	4.79	1263	485	869	363
RRELU	1.84	4.47	3.96	5.85	4.03	1661	385	1892	313
SOFTSHRINK	18.17	18.30	18.17	18.30	18.23	1688	479	1834	345

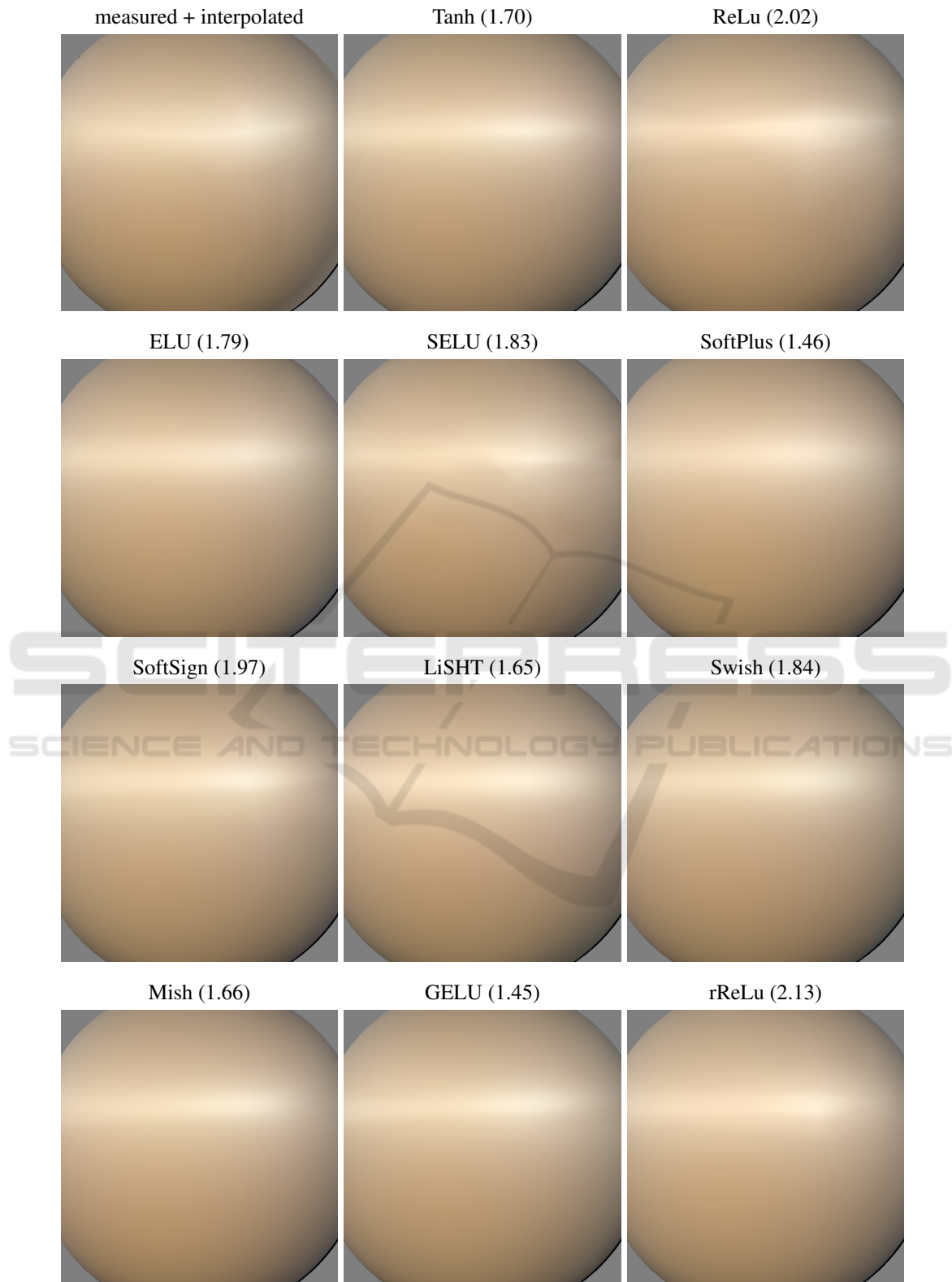


Figure 5: Spruce rendered modeling results (model **15–30–20** with *va-ia*) with rendering errors.

artifacts are more visible on lustrous materials (Fig. 5) than on the matted materials.

Tab. 3 shows the average model learning time of specific activation functions in seconds. Apart from the fastest linear activation function, the fastest nonlinear functions are Sigmoid, Exponential, Tanh, ReLU, ELU, and SELU. SoftSign is only 12% slower than the fastest Sigmoid function. SoftShrink evaluation has the most time expensive evaluation (209%).

Tabs. 2,3 show that the best modeling interpolation is achieved if we teach the model from all viewing and illumination angles (Fig. 5). The modeling error results of the smaller NN-BRDF model are more stable during training data subsampling. Tab. 2 shows a modeling improvement if we teach the model from all illumination angles but only sixth viewing angles (*vs-ia*) in comparison with all viewing angles and only sixth illumination angles (*va-is*) for both models and the spruce wood. The maximal  $\Delta\bar{\epsilon}$  error is 2.6 (10%). If the models are learned from only sixth illumination and viewing angles (*vs-is*) (3% of measurements), the SoftSign activation function is the most robust with an average error increase  $\Delta\bar{\epsilon} = 3.4$ , Tanh is only slightly worse.

Fig. 1 illustrates the estimated NN-BRDF results and their enhanced pixelwise differences from the measured spruce and green cloth anisotropic BRDFs. The median precision over all activation functions for both compared BRDF's (Tabs. 2,3) is in the range of the average spectral modeling error 2.0 – 12.4 and (4.3% – 19.5%) for larger and smaller model, respectively. The performance of our BRDF model was also compared with six anisotropic analytical BRDF models. Their spectral mean BRDF interpolation error for the spruce material is in the range of 14 for the best Phong model (Phong, 1975) to 108 for the worst Edwards model (Edwards et al., 2006).

For additional and more detailed results see <https://mosaic.utia.cas.cz/23GRAPP/>.

## 5 CONCLUSION

The presented anisotropic neural NN-BRDF models allow us to accurately model anisotropic and isotropic BRDF for various materials with less than 2.8% average error increase from only 3% of the original measurements. This almost 97% measurement reduction saves measurement costs and time significantly. The models learn from more informative BTF data than usually restricted BRDF measurements.

The best activation function for all tested materials is SoftSign, followed by Tanh, GELU, ELU, and SELU from all tested twenty activation functions.

Visual quality comparison of our NN-BRDF models confirms the same ranking. The non-smooth functional parts of activation functions produce apparent visual defects. These significant artifacts are visible if mapped on curved object surfaces; thus, they cannot be used for realistic NN-BRDF modeling.

The extensive UTIA BTF / BRDF database verified all modeling results with stable results on varied wood species and several other materials. The model results are also illustrated on textile and spruce anisotropic materials. The presented model can reconstruct the fully measured angular BRDF hemisphere from sparse measurements and predict an unmeasured, high-resolution BRDF hemisphere from a low-resolution measurement net. We have also favorably compared our numerical as well as visual results with several analytical previously published BRDF models and planned to publish these results elsewhere. The presented models can be used directly as a fast replacement of a BRDF, comparable to fast analytic BRDF models, in a rendering engine. They simultaneously offer a high compression rate and interpolation of unmeasured angles.

## ACKNOWLEDGMENTS

The Czech Science Foundation project GAČR 19-12340S supported this research.

## REFERENCES

- Ashikhmin, M. and Shirley, P. (2000). An anisotropic phong brdf model. *Journal of graphics tools*, 5(2):25–32.
- Bell, S., Upchurch, P., Snavely, N., and Bala, K. (2015). Material recognition in the wild with the materials in context database. In *Proceedings of the IEEE conference on computer vision and pattern recognition*, pages 3479–3487.
- Blinn, J. F. (1977). Models of light reflection for computer synthesized pictures. In *Proceedings of the 4th annual conference on Computer graphics and interactive techniques*, pages 192–198. ACM Press.
- Chen, Z., Nobuhara, S., and Nishino, K. (2021). Invertible neural brdf for object inverse rendering. *IEEE Transactions on Pattern Analysis and Machine Intelligence*, pages 1–1.
- Cook, R. L. and Torrance, K. E. (1982). A reflectance model for computer graphics. *ACM Transactions on Graphics (TOG)*, 1(1):7–24.
- Dahlan, H. A. and Hancock, E. R. (2016). Absorptive scattering model for rough laminar surfaces. In *2016 23rd International Conference on Pattern Recognition (ICPR)*, pages 1905–1910. IEEE.

- Edwards, D., Boulos, S., Johnson, J., Shirley, P., Ashikhmin, M., Stark, M., and Wyman, C. (2006). The halfway vector disk for brdf modeling. *ACM Transactions on Graphics (TOG)*, 25(1):1–18.
- Fan, J., Wang, B., Hašan, M., Yang, J., and Yan, L.-Q. (2021). Neural brdfs: Representation and operations. *arXiv preprint arXiv:2111.03797*.
- Gibert, X., Patel, V. M., and Chellappa, R. (2015). Material classification and semantic segmentation of railway track images with deep convolutional neural networks. In *2015 IEEE International Conference on Image Processing (ICIP)*, pages 621–625. IEEE.
- Haindl, M. and Filip, J. (2013). *Visual Texture*. Advances in Computer Vision and Pattern Recognition. Springer-Verlag London, London.
- Haindl, M., Filip, J., and Vávra, R. (2012). Digital material appearance: the curse of tera-bytes. *ERCIM News*, (90):49–50.
- Haindl, M., Mikeš, S., and Kudo, M. (2015). Unsupervised surface reflectance field multi-segmenter. In Azopardi, G. and Petkov, N., editors, *Computer Analysis of Images and Patterns*, volume 9256 of *Lecture Notes in Computer Science*, pages 261 – 273. Springer International Publishing.
- Lafortune, E., Foo, S., Torrance, K., and Greenberg, D. (1997). Non-linear approximation of reflectance functions. In *ACM SIGGRAPH 97*, pages 117–126. ACM Press.
- Minnaert, M. (1941). The reciprocity principle in lunar photometry. *The Astrophysical Journal*, 93:403–410.
- Ngan, A., Durand, F., and Matusik, W. (2005). Experimental analysis of brdf models. In *Proceedings of the Sixteenth Eurographics Conference on Rendering Techniques*, EGSR '05, page 117–126, Goslar, DEU. Eurographics Association.
- Nielsen, J. B., Jensen, H. W., and Ramamoorthi, R. (2015). On optimal, minimal brdf sampling for reflectance acquisition. *ACM Trans. Graph.*, 34(6):186:1–186:11.
- Oren, M. and Nayar, S. K. (1994). Generalization of lambert's reflectance model. In *Proceedings of the 21st annual conference on Computer graphics and interactive techniques*, pages 239–246.
- Phong, B. T. (1975). Illumination for computer generated pictures. *Communications of the ACM*, 18(6):311–317.
- Ragheb, H. and Hancock, E. R. (2008). A light scattering model for layered dielectrics with rough surface boundaries. *International Journal of Computer Vision*, 79(2):179–207.
- Schlick, C. (1993). A customizable reflectance model for everyday rendering. In *Fourth Eurographics Workshop on Rendering*, pages 73–83. Paris, France.
- Shamir, G. I., Lin, D., and Coviello, L. (2020). Smooth activations and reproducibility in deep networks. *arXiv preprint arXiv:2010.09931*.
- Strauss, P. S. (1990). A realistic lighting model for computer animators. *IEEE Computer Graphics and Applications*, 10(6):56–64.
- Sztrajman, A., Rainer, G., Ritschel, T., and Weyrich, T. (2021). Neural brdf representation and importance sampling. In *Computer Graphics Forum*, volume 40, pages 332–346. Wiley Online Library.
- Torrance, K. E. and Sparrow, E. M. (1966). Off-specular peaks in the directional distribution of reflected thermal radiation. *Journal of Heat Transfer*, 6(7):223–230.
- Varma, M. and Zisserman, A. (2009). A statistical approach to material classification using image patch exemplars. *IEEE Transactions on Pattern Analysis and Machine Intelligence*, 31(11):2032–2047.
- von Helmholtz, H. (1867). *Handbuch der physiologischen Optik*, volume 9. Leipzig: Voss.
- Ward, G. (1992). Measuring and modeling anisotropic reflection. *Computer Graphics*, 26(2):265–272.
- Xu, Z., Nielsen, J. B., Yu, J., Jensen, H. W., and Ramamoorthi, R. (2016). Minimal brdf sampling for two-shot near-field reflectance acquisition. *ACM Trans. Graph.*, 35(6).
- Zheng, C., Zheng, R., Wang, R., Zhao, S., and Bao, H. (2021). A compact representation of measured brdfs using neural processes. *ACM Trans. Graph.*, 41(2).